Redox Biology 36 (2020) 101632

Contents lists available at ScienceDirect

Redox Biology

journal homepage: www.elsevier.com/locate/redox

Melatonin sensitises shikonin-induced cancer cell death mediated by oxidative stress via inhibition of the SIRT3/SOD2-AKT pathway

Mengling Li [a], Chengai Wu [b], Jibran Sualeh Muhammad [c], Dan Yan [d], Koichi Tsuneyama [e], Hideki Hatta [f], Zheng-Guo Cui [a,g,1,*], Hidekuni Inadera [a,1,**]

[a] Department of Public Health, Graduate School of Medicine and Pharmaceutical Sciences, University of Toyama, 2630 Sugitani, Toyama, 930-0194, Japan
[b] Institute of Orthopaedic Trauma, Xicheng District Xinjiekou East Street on the 31st, Beijing, 100035, China
[c] Department of Basic Medical Sciences, College of Medicine, University of Sharjah, Sharjah, 27272, United Arab Emirates
[d] Department of Pharmacy, Beijing Shijitan Hospital, Capital Medical University, Beijing, China
[e] Department of Pathology and Laboratory Medicine, Institute of Biomedical Sciences, Tokushima University Graduate School, Tokushima, Japan
[f] Department of Diagnostic Pathology, Graduate School of Medicine and Pharmaceutical Sciences, University of Toyama, 2630 Sugitani, Toyama, 930-0194, Japan
[g] Department of Environmental Health, University of Fukui School of Medical Science, University of Fukui, Fukui, 910-1193, Japan

ARTICLE INFO

Keywords:
Melatonin
SIRT3/SOD2
Apoptosis
Reactive oxygen species
AKT
Shikonin

ABSTRACT

Recent research suggests that melatonin (Mel), an endogenous hormone and natural supplement, possesses anti-proliferative effects and can sensitise cells to anti-cancer therapies. Although shikonin (SHK) also possesses potential anti-cancer properties, the poor solubility and severe systemic toxicity of this compound hinders its clinical usage. In this study, we combined Mel and SHK, a potentially promising chemotherapeutic drug combination, with the aim of reducing the toxicity of SHK and enhancing the overall anti-cancer effects. We demonstrate for the first time that Mel potentiates the cytotoxic effects of SHK on cancer cells by inducing oxidative stress via inhibition of the SIRT3/SOD2-AKT pathway. Particularly, Mel-SHK treatment induced oxidative stress, increased mitochondrial calcium accumulation and reduced the mitochondrial membrane potential in various cancer cells, leading to apoptosis. This drug combination also promoted endoplasmic reticulum (ER) stress, leading to AKT dephosphorylation. In HeLa cells, Mel-SHK treatment reduced SIRT3/SOD2 expression and SOD2 activity, while SIRT3 overexpression dramatically reduced Mel-SHK-induced oxidative stress, ER stress, mitochondrial dysfunction and apoptosis. Hence, we propose the combination of Mel and SHK as a novel candidate chemotherapeutic regimen that targets the SIRT3/SOD2-AKT pathway in cancer.

1. Introduction

The incidence of cancer and associated mortality is increasing rapidly worldwide, with an estimated 18 million new cases and 9.5 million cancer-related deaths in 2018 [1]. Although surgery, chemotherapy, and radiotherapy are the mainstays of cancer treatment, elderly patients and those with advanced-stage cancer experience a worse prognosis, more adverse effects, and increased tumour recurrence [2]. To address these challenges, improvements in existing chemotherapies and treatments that target specific oncogenic pathways are needed. In one promising approach, natural compounds known to possess anti-cancer properties could be potentiated when combined with non-toxic dietary supplements to minimise toxicity and enhance anti-cancer efficacy.

The hormone melatonin (Mel, *N*-acetyl-5-methoxytryptamine), previously thought to be secreted only by the pineal gland, is now known to be synthesised by the mitochondria in every cell of almost every organ of the body [3]. Interestingly, artificial night-time light disrupts Mel production and the normal circadian rhythm, which is reported to contribute to the initiation, promotion, and progression of cancers [4,5]. The endogenous production and virtually non-toxic nature of Mel render it an ideal chemotherapeutic option. Shikonin (SHK), an active natural

* Corresponding author. Department of Environmental Health, University of Fukui School of Medical Science, University of Fukui, Fukui, 910-1193, Japan.
** Corresponding author. Department of Public Health, Graduate School of Medicine and Pharmaceutical Sciences, University of Toyama, 2630 Sugitani, Toyama, 930-0194, Japan.
E-mail addresses: sai@u-fukui.ac.jp (Z.-G. Cui), inadera@med.u-toyama.ac.jp (H. Inadera).
[1] Zheng-Guo Cui and Hidekuni Inadera contributed equally.

https://doi.org/10.1016/j.redox.2020.101632
Received 2 April 2020; Received in revised form 3 June 2020; Accepted 29 June 2020
Available online 2 July 2020

plant extracts, has recently attracted much attention in the development of new anti-cancer therapeutic strategies [6]. In particularly, SHK induces reactive oxygen species (ROS), which play upstream roles in mitochondria-mediated apoptosis and cancer cell death [7,8]. Unfortunately, the poor solubility and severe systemic toxicity of SHK hinder its clinical use as an anti-cancer drug [9]. Although recent studies have demonstrated that combinations of Mel with various anti-cancer drugs sensitised cancer cells and enhanced apoptosis by reducing cell viability and growth [10–12], the anti-cancer effects of Mel combined with SHK have never been explored.

Sirtuin-3 (SIRT3) regulates intracellular metabolism mainly by modulating mitochondrial oxidative stress [13]. In mitochondria, SIRT3 primarily deacetylates stress-responsive proteins and regulates mitochondrial membrane integrity and energy homeostasis [14]. Additionally, SIRT3 regulates superoxide dismutase 2 (SOD2) by deacetylating and activating the SOD2 transcription factor FOXO3a, or by directly deacetylating and activating SOD2 dismutase activity. SOD2 then catalyses the neutralisation of superoxide conversion into water and hydrogen peroxide [15,16]. Decreased SIRT3 expression enhances ROS-mediated oxidative damage, suggesting that SIRT3 inhibitors may be therapeutically beneficial. Furthermore, studies demonstrating the role of SIRT3-induced apoptosis in cancer cells [17,18] suggest that combinations such as Mel and SHK might function via inhibition of the SIRT3-SOD2 pathway to induce cancer cell death.

In this study, we explored the ability of Mel to augment the anti-cancer effect of SHK. We demonstrated, for the first time, that Mel-SHK induced endoplasmic reticulum (ER) stress and increased ROS production by inhibiting the SIRT3-SOD2 and AKT pathway, and reduced cell growth and survival in various cancers.

2. Materials and methods

2.1. Chemicals and inhibitors

Mel, SHK, *N*-acetyl-cysteine (NAC, ROS scavenger), 4-Bromo-Resveratrol (4-BR, SIRT inhibitor), *N*-Benzyloxycarbonyl-Val-Ala-Asp(O–Me) fluoromethyl ketone (Z-VAD-FMK, caspase inhibitor), 4-phenylbutyric acid (4-PBA, ER stress inhibitor), LY 294002 (PI3K inhibitor), Necrostatin-1 (Nec-1, a specific inhibitor of RIP1 kinase), necrosulfonamide (NSA, a specific inhibitor of necrosis downstream of RIP3 activation), U0126 (MEK-1/2 inhibitor), a JNK inhibitor (JNK-IN-8) and a p38 inhibitor (SB203580) were all purchased from Sigma-Aldrich (St. Louis, MO, USA) and were solubilised as recommended.

2.2. Cell culture and treatment

A human histiocytic lymphoma (U937; RRID: CVCL_0007) cell line was obtained from the Human Sciences Research Resources Bank (Tokyo, Japan) and was cultured using RPMI-1640 medium, supplemented with 10% heat-inactivated fetal bovine serum (FBS) at 37 °C, in humidified air with 5% CO_2. Additionally, human papillomavirus-related endocervical adenocarcinoma (HeLa; RRID: CVCL_0030), human hepatoblastoma (Hep-G2; RRID: CVCL_0027), human gastric cancer (AGS; RRID: CVCL_0139), human breast adenocarcinoma (MCF-7; RRID: CVCL_0031), human colon adenocarcinoma (SW480; RRID: CVCL_0546), human lung adenocarcinoma (A549; RRID: CVCL_0023), baby hamster kidney fibroblasts (BHK; RRID: CVCL_ 1915), murine fibroblast (NIH3T3; RRID: CVCL_0594), and human skin keratinocytes (HaCaT; RRID: CVCL_0058) cell lines were obtained from the Japan Cancer Research Resources Bank (Tokyo, Japan). African green monkey kidney (Vero; ATCC: CCL_81) cells were obtained from the American Type Culture Collection (Manassas, VA, USA). All the cell lines were mycoplasma-free cells and were authenticated using short tandem repeat (STR) genotyping within the last three years and were verified to be identical with the STR profile in comparing databases. These cells were grown in RPMI-1640 or Dulbecco's Modified Eagle's Medium (DMEM), containing 10% heat-inactivated FBS, and maintained in a humidified incubator at 37 °C with 5% CO_2. U937 and HeLa cells were used more extensively, and target molecules and pathways were investigated mainly in the latter. Cells were seeded into dishes or plates overnight according to experimental requirements, and were treated with the indicated concentrations of SHK with or without Mel. Inhibitors were pre-treated for 1 h before co-treatment with SHK and Mel.

2.3. MTT assay

The MTT (3-4,5-dimethyl-2-thiazolyl)-2,5-diphenyl-2-H-tetrazolium bromide) assay was used to evaluate cell viability. Cells were seeded into 96-well plates at 4×10^3 cells/well overnight. Briefly, MTT (5 mg/mL) solution was added to 96-well plates at 20 μL/well followed by incubation for 4 h at 37 °C, and DMSO (dimethyl sulfoxide) was added at 150 μL/well. The absorbance was measured at 490 nm on a microplate reader as reported previously [19]. Eight parallel wells were used for each concentration.

2.4. Lactate dehydrogenase (LDH)-based cytotoxicity assay

The cytotoxicity was measured by quantitating the release of LDH. Following incubation, the media was collected and centrifuged for 5 min. The supernatants were collected and added to a 96-well plate at 50 μL per well for LDH measurements, and then reaction buffer was added at the same volume. The assay plates were then incubated at room temperature in the dark for 20 min. Finally, 100 μL of stop buffer (diluted with PBS at 1:1) was added to each of the assay wells. The total volume in each well was 200 μL. The absorbance was measured at 570 nm on a microplate reader, as reported previously [20].

2.5. Assessment of DNA fragmentation

The cells were harvested 6 h after the treatment, and lysed with 200 μL of lysis buffer (10 mmol/L Tris, 1 mmol/L EDTA, and 0.1% NP-40, pH 7.5) and centrifuged at 13,000 g for 10 min to separate intact from fragmented chromatin. The supernatant-containing fragmented DNA and the pellet were precipitated overnight at 4 °C in 12.5% trichloroacetic acid (TCA). The DNA precipitates were hydrolysed by heating to 90 °C for 20 min in 5% TCA overnight. For quantification of the fragmented DNA, the absorbance at 600 nm was measured (Beckman DU-50 Spectrophotometer; Beckman Coulter, Brea, CA, USA) with diphenylamine (DPA) reagent (0.15 g DPA, 0.15 mL H_2SO_4, and 0.05 mL acetaldehyde per 10 mL glacial acetic acid). "Percent fragmentation" refers to the ratio of DNA in the supernatant ("fragmented") to the total DNA recovered in both the supernatant and pellet ("fragmented plus intact").

2.6. Drug combination assays

Drug combinations were evaluated using the combination index (CI) method described by Chou and Talalay [21,22]. Briefly, the data of cell viability, as evaluated above, were analysed using CompuSyn software (ComboSyn, Inc., Paramus, NJ, USA) [21] to calculate the synergy between Mel and SHK (Mel:SHK = 2:1 in U937, AGS cells; 1:2 in HeLa, MCF7, A549 cells; 1:4 in HepG2 cells; and 1:1 in SW480 cells). The resulting CI theorem of Chou-Talalay offers a quantitative definition for additive effect (CI = 1), synergism (CI < 1), and antagonism (CI > 1) in drug combinations.

2.7. IC_{50} shift assays

The IC_{50} shift assay was used to determine the IC_{50} (i.e., the drug concentration that results in a 50% inhibition of activity) following SHK treatment, in the absence and presence of Mel. Briefly, cells were treated with various concentrations of SHK or co-treated with 2 mM Mel. After 6 h (U937) or 24 h, cellular inhibition was calculated. The curve-fit lines

were generated using a non-linear curve fitting (regression) analysis in GraphPad Prism 5 (GraphPad Software, La Jolla, CA, USA) and the IC_{50} shift was calculated.

2.8. Apoptosis detection with flow cytometry

The cells were harvested after 24 h of treatment and stained with fluorescein isothiocyanate-labelled annexin V (Annexin V/FITC) and propidium iodide (PI) for 30 min, prior to being analysed using a flow cytometry according to the manufacturer's instructions.

2.9. Cell colony formation

Cells (2×10^2 per well) were seeded in 6-well plates and were cultivated in indicated media for 10–14 days after treatment. Subsequently, the media was removed, cells were washed twice in PBS and were fixed using 4% paraformaldehyde for 1 h and stained with crystal violet for 40 min at room temperature. Plates were thoroughly washed with water and air-dried at room temperature.

2.10. Western blotting and immunoprecipitation (IP)

After the desired treatment, cells were washed with PBS three times, and the total protein was extracted using RIPA lysis buffer or IP buffer containing protease and phosphatase inhibitors. The cell extracts were centrifuged at 13,000 rpm at 4 °C for 15 min. The supernatants were transferred to 1.5 mL Eppendorf tubes. The concentrations of the proteins were measured using the Bradford Protein Assay Kit at 560 nm on a microplate reader. Twenty micrograms of protein per sample were electrophoresed at 18 mA for 90 min, followed by transfer to PVDF membranes (MilliporeSigma, Burlington, MA, USA) at 15 V, 0.15 A for 90 min. Next, the membranes were blocked in 5% nonfat milk in TBST (150 mM NaCl, 50 mM Tris at pH 7.5, 0.1% Tween-20) for 2 h, and the specific primary antibody was incubated overnight at 4 °C. After TBST washing, the horseradish peroxidase (HRP)-labelled secondary antibody was added for 2 h at room temperature. Finally, the target proteins were detected using an enhanced chemiluminescent (ECL) kit (Amersham Biosciences, Buckinghamshire, UK) in accordance with the manufacturer's instructions. The band densities were measured using Image Studio Lite (LI-COR Biosciences, Lincoln, NE, USA).

2.11. Detection of ROS levels

Alterations in the ROS levels were determined by dihydroethidium (DHE) staining (Molecular Probes, Eugene, OR, USA), which exhibits blue-fluorescence in the cytosol and can be oxidized by ROS in cells to form ethidium oxide, which can be incorporated into chromosomal DNA to produce red-fluorescent. Briefly, the cells were incubated with 4 μM DHE for 15 min at 37 °C. After washing twice with PBS, the population of ethidium bromide-stained cells was measured using FACS Canto II (EPICS XL, Beckman-Coulter, Miami, FL, USA and FACS Canto II, BD Biosciences, Mississauga, ON, USA) as the fraction of cells producing intracellular ROS, according to the manufacturer's protocol.

2.12. SOD2 activity

SOD2 activity was measured using the SOD Assay kit and a water-soluble tetrazolium salt (WST)-1 as a substrate, in accordance with the manufacturer's protocol (Dojindo Molecular Technology, Kumamoto, Japan). Briefly, the SOD activity of each immunoprecipitated protein was indicated by the inhibition of the WST-1 reduction rate. Potassium cyanide (1 mM) was added to the lysate (10 μg of total protein) during the assay to inhibit SOD1 and SOD3. Absorbance was measured at 450 nm on a microplate reader, as reported previously [23].

2.13. Estimation of mitochondrial free calcium ions

The calcium probe Rhod 2-AM (Sigma-Aldrich, St. Louis, MO, USA) was used to determine the effects of individual and combined treatments on mitochondrial calcium homeostasis. Cells were harvested after 12 h of treatment and were stained with 5 μM Rhod 2-AM for 30 min. The calcium fluorescence intensity was measured using a flow cytometry at excitation and emission maxima of 557 and 581 nm, respectively.

2.14. Sub-G1 analysis

Cells were harvested after 24 h of treatment and centrifuged at 200×*g* at room temperature for 5 min. Cell pellets were suspended in 100 μL PBS, fixed with 75% (v/v) cold ethanol for 2 h and stained with a PI solution containing DNase-free RNase A for 30 min at room temperature in the dark. Cells were analysed using a flow cytometry according to the manufacturer's instructions.

2.15. Mitochondrial membrane potential

Tetramethylrhodamine methyl ester perchlorate (TMRM) is a cationic fluorophore used widely to stain the mitochondria and mitochondrial matrices. Cells were harvested at an indicated time after treatment and exposed to 10 nM TMRM (Molecular Probes, Eugene, Oregon, USA) in 1 mL of PBS plus 1% FBS for 15 min at 37 °C. The percentage of cells with a low mitochondrial membrane potential (MMP) was detected by flow cytometry according to the manufacturer's instructions.

2.16. Wound healing assay

Cells (3×10^5 per well) were seeded in 6-well plates overnight to ensure at least 90% confluency. Then, the cellular layer was scratched with a sterile micropipette tip (200 μL) to create a free-cell area. Non-adherent cells were washed three times using an FBS-free medium. The migration distance was measured on the images captured at 24 h, 48 h and 72 h after SHK treatment with or without Mel using Image J software (National Institute for Health, Bethesda, MD, USA). The migration rate (MR) was calculated as $[(A - B)/A] \times 100$, where A is the width at 0 h, and B is the width of indicated time at 24 h, 48 h and 72 h, respectively.

2.17. Immunofluorescence

Cells were seeded on glass coverslips. After treatment, the cells were incubated with an anti-SIRT3 or anti-SOD2 antibody overnight at 4 °C and stained with an Alexa Fluor 647-conjugated goat anti-rabbit secondary antibody. Nuclei were counterstained with Hoechst 33258. Immunofluorescence images were acquired using an LSM 780 confocal microscope (Carl Zeiss AG, Oberkochen, Germany).

2.18. Plasmids and transfection

The SIRT3-Flag plasmid was purchased from Addgene (Watertown, MA, USA). HeLa cells cultured in DMEM for 24 h were transfected with a SIRT3-Flag plasmid using the Amaxa® Cell Line Nucleofector® Kit according to the manufacturer's instructions. After 24 h, cells were processed for immunoblotting and other assays according to the above-described experimental requirements.

2.19. Statistical analysis

All experiments were performed in biologically independent triplicates. Data are presented as means ± standard errors of the means (SEM). Statistical analyses were performed using CompuSyn and GraphPad Prism 5. The values of R (CompuSyn) and R^2 (Graphpad) were

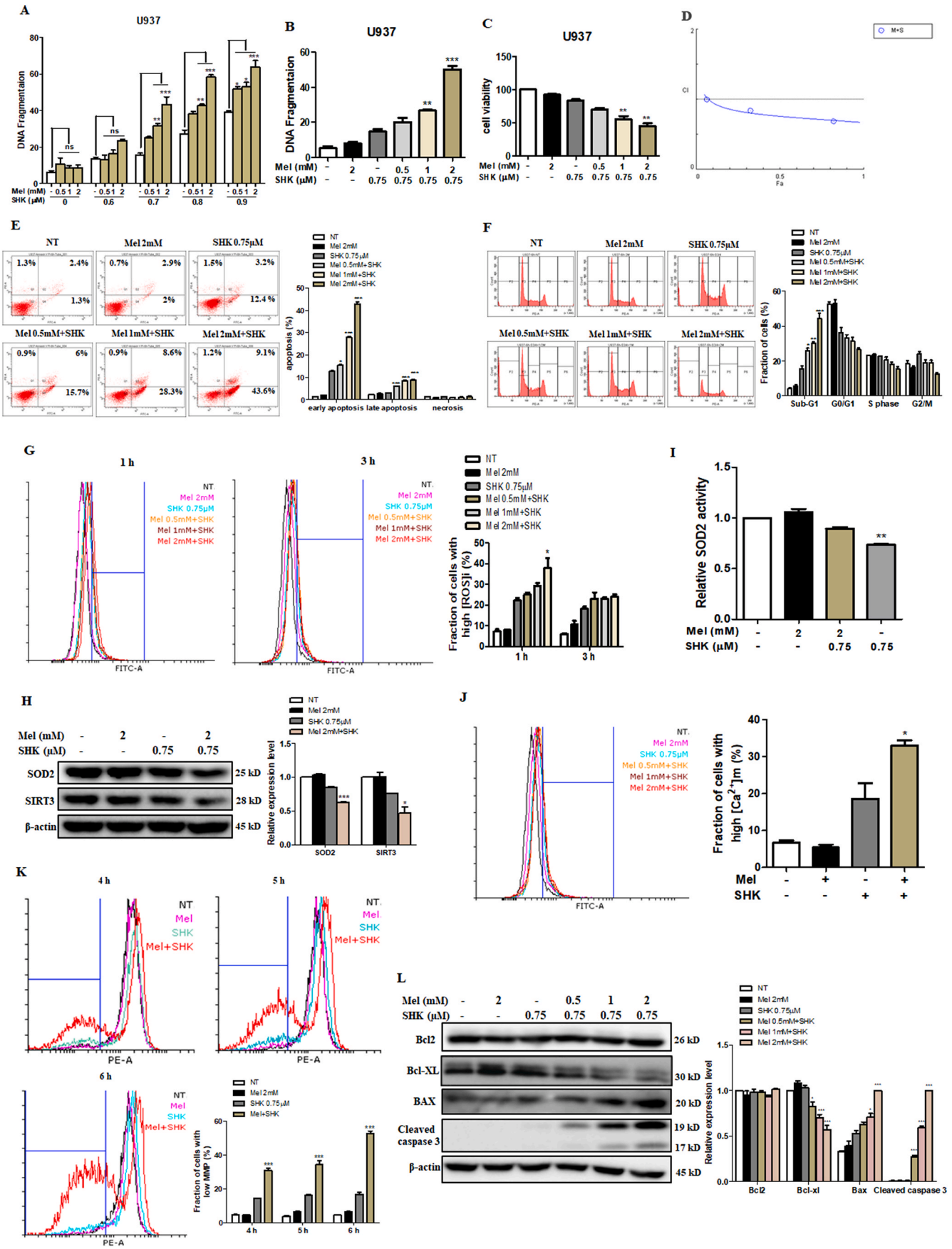

(caption on next page)

Fig. 1. The melatonin-shikonin (Mel-SHK) combination exerts strong anti-cancer activities and downregulates SIRT3/SOD2 in U937 cells. U937 cells were treated with melatonin (Mel, 0–2 mM) or shikonin (SHK, 0–0.9 μM) alone or in combination for 6 h unless otherwise indicated. (A) DNA fragmentation was assessed. The histogram depicts the percentage of DNA fragmentation in cells treated with SHK alone (white bars) or in combination with Mel at various concentrations. The effects of SHK (0.75 μM) and concomitant dose-dependent effect of Mel (0–2 mM) were investigated with respect to (B) DNA fragmentation, (C) cell viability, (D) Combination Index (CI), (E) apoptosis [Annexin V/propidium iodide (PI) double-staining] and (F) hypodiploid (sub-G1) DNA content. (G) Cells with high levels of reactive oxygen species (ROS) were evaluated at 1 h and 3 h post-treatment. (H) SOD2 and SIRT3 protein expression levels were analysed by western blotting 1 h after treatment with Mel and SHK alone or in combination. The bar graph depicts the relative expression levels compared to SHK treatment alone. (I) Relative analysis of SOD2 activity. (J) Mitochondrial calcium (Ca^{2+}) levels at 1 h and (K) mitochondrial membrane potential (MMP) at 4 h, 5 h and 6 h post-treatment. (L) Western blotting analysis of pro-apoptotic and anti-apoptotic protein expression. Flow cytometry data are presented as histograms and bar graphs. Relative protein expression was calculated for all western blots, using actin for normalisation and as a loading control. One representative figure from at least three independent experiments is shown for each assay. The data in each bar graph are presented as the means ± standard errors of the means (SEM). *$P < 0.05$, **$P < 0.01$, and ***$P < 0.001$ relative to SHK treatment alone.

used to describe the goodness-of-fit of linear and non-linear regression trend lines, respectively. Image J was used to calculate the relative protein expression from Western blot images. Analyses of different treatment groups were performed by one-way analysis of variance (ANOVA) or two-way ANOVA using Tukey's post hoc test. A value of $P < 0.05$ was considered statistically significant.

3. Results

3.1. Mel-SHK-induced anti-cancer activity and SIRT3-SOD2 downregulation in U937 cells

U937 cells were treated with varying levels of SHK (0–0.9 μM) and Mel (0–2 mM), the latter had no obvious effect on DNA fragmentation. However, dose-dependent increases in DNA fragmentation were observed in U937 cells treated with Mel-SHK, compared to cells treated with SHK alone (Fig. 1A). A combination of 0.75 μM SHK and 2 mM Mel exerted the most optimal effects on DNA fragmentation and cell viability (~50%; Fig. 1B and C) and disrupted cell morphology (phase-contrast microscopy; Fig. S1A). Combination Index (CI) values were calculated and depicted in Fig. 1D; CI values < 1 are considered to be synergistic. The promotion of SHK by Mel was observed, since a 1.84-fold shift for SHK was observed in the IC_{50} shift assay (Fig. S1B). To understand the timing of Mel treatment on cancer cell sensitization, we evaluated the effect of pre-treatment of the cells with Mel (0.5, 1, 2 mM) for 1 h followed by SHK (0.75 μM for U937 and 3 μM for HeLa) treatment. For both the cell types, cell viability was reduced significantly and dose-dependently (Fig. S1C). In addition, we compared the differences in cell viability after Mel pre-treatment followed by SHK treatment, versus simultaneous Mel and SHK treatment. The results showed that, when compared to combined treatment, pre-treatment of Mel for 1 h followed by SHK has almost similar effects on cancer cell sensitisation. For both U937 and HeLa cells, the reduction in cell viability was the same without any significant difference amongst the two ways of treatment (Fig. S1D). Hence, for further experiments only the combination treatment was used.

Mel-SHK significantly enhanced apoptosis, as evidenced by an increase in Annexin V-FITC-positivity and sub-G1 phase accumulation of approximately 30% vs. SHK treatment alone (Fig. 1E and F). Activation of apoptosis-related proteins and ROS generation are key apoptosis triggers [24]. Mel-SHK treatment for 1 h showed a sharp increase in the levels of ROS production (Fig. 1G), which was associated with a significant decrease in SIRT3/SOD2 expression and a decrease in relative SOD2 activity compared with SHK alone (Fig. 1H and I). Additionally, Mel-SHK treatment induced mitochondrial calcium overload and an increased number of cells with a low MMP over time (Fig. 1J and K). Furthermore, combined treatment also inhibited Bcl-xL expression, enhanced Bax expression, and induced caspase-3 cleavage in U937 cells (Fig. 1L).

3.2. Mel-SHK-induced cytotoxicity and caspase activation in solid cancer cell lines

Mel-SHK treatment induced a significant, dose-dependent reduction in cell viability and enhanced cytotoxicity in 4 solid cancer cell lines (AGS, MCF7, SW480, and HeLa; Fig. 2A–D), but exerted less significant effects in HepG2 and A549 cells (Fig. 2E and F). We also calculated the CI values, and the CI theorem of Chou-Talalay offers quantitative definition for additive effect (CI = 1), synergism (CI < 1), and antagonism (CI > 1) in drug combinations (Fig. 2 A–F). Furthermore, the promotion of SHK by Mel was further demonstrated using IC_{50} shift assay, as shown in Fig. S2A. Additionally, Mel-SHK upregulated the levels of cleaved caspase-3 and/or PARP in AGS, MCF7, and SW480 cells (Fig. 2G–I). HeLa cells, which are the oldest and most commonly used human cell line [25], were selected for a detailed analysis of the pathways involved in Mel-SHK-induced cancer cell death in later experiments.

3.3. Mel- SHK-induced cell growth inhibition and apoptosis in HeLa cells

To understand the anti-cancer properties of Mel sensitised SHK, several aspects of carcinogenesis were investigated. We confirmed that Mel (0–2 mM) potentiates the deleterious effects of SHK (3 μM) on cancer cell viability and increases cytotoxicity in a dose-dependent manner (Fig. 3A and B) via phase-contrast microscopy (Fig. S2B and C). We conducted a clonogenic assay for up to 10 days after treatment to evaluate the long-term effects of Mel-SHK on cancer cell survival. Notably, the number of cells, as well as the sizes of colonies in Mel-SHK-treated groups, appeared fewer and smaller, respectively, compared with Mel or SHK individual treatment, further confirming the anti-proliferative effect of this combination (Fig. 3C). Additionally, combined treatment significantly increased apoptosis and sub-G1 phase accumulation (Fig. 3D and E). As shown in Fig. 3F, Mel-SHK treatment decreased the expression of CDC25C, an important cell cycle regulator [26], and the dephosphorylation of cdc2 (Tyr15) and CHK1. Although p-Rb (Ser795) downregulation was noted in Mel-SHK-treated cells, no change in the p-P53 level was observed.

We also used a wound healing assay to assess the effect of Mel-SHK on cell migration. Combined treatment significantly inhibited HeLa cell migration, as indicated by an approximately 60% reduction in scratch width vs. approximately 80% and 90% reductions in SHK- and Mel-treated cells at 72 h post treatment (Fig. 3G). We further determined that Mel-SHK significantly inhibited the expression of matrix metalloproteinases-2 (MMP-2) and MMP-9, which are strongly associated with cancer metastasis (Fig. 3H) [27].

Next, we analysed apoptosis-related proteins by western blotting to investigate the effect of Mel-SHK on apoptotic HeLa cell death. Notably, combined treatment downregulated the anti-apoptotic proteins Bcl-xL and XIAP while promoting caspase-3 and PARP cleavage, suggesting the initiation of caspase-mediated apoptosis. Mel-SHK co-treatment also significantly downregulated UHRF1, a major factor in the G1/S phase transition and DNA damage checkpoint (Fig. 3I) [28].

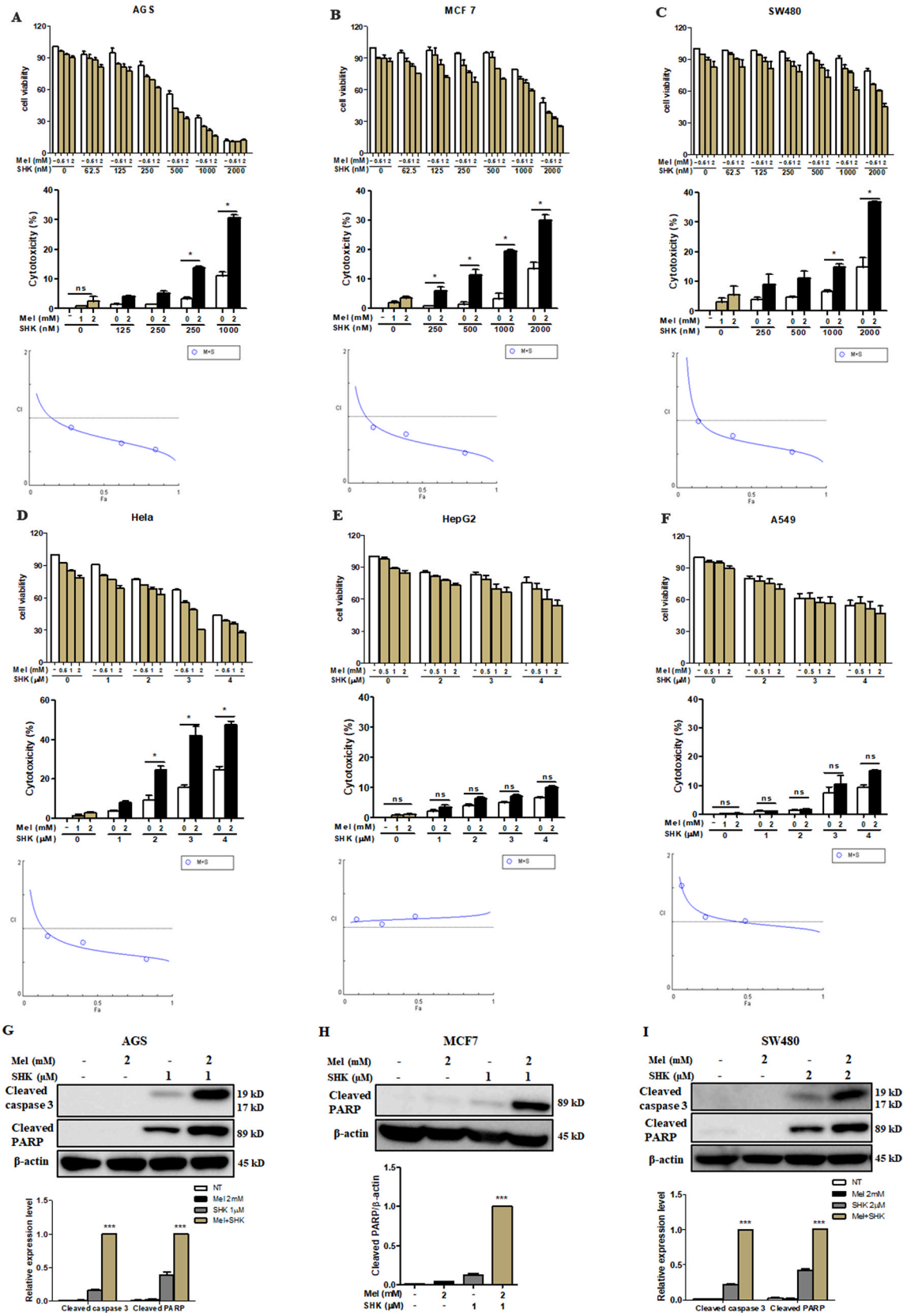

Fig. 2. Treatment with melatonin-shikonin (Mel-SHK) enhances cytotoxicity and caspase activation in solid cancer cell lines. (A) AGS, (B) MCF7, (C) SW480, (D) HeLa, (E) HepG2, and (F) A549 cells were treated with Mel and/or SHK at various concentrations. Caspase 3 and/or PARP cleavage was investigated in (G) AGS, (H) MCF7 and (I) SW480 cells. In all experiments, the treatment duration was 24 h. The relative protein expression was calculated, and one representative figure from at least three independent experiments is shown. Actin was used for normalisation and as a loading control. The data in each bar graph are presented as the means ± SEM (n = 3). ns: not significant, *P < 0.05 and ***P < 0.001 relative to SHK treatment alone.

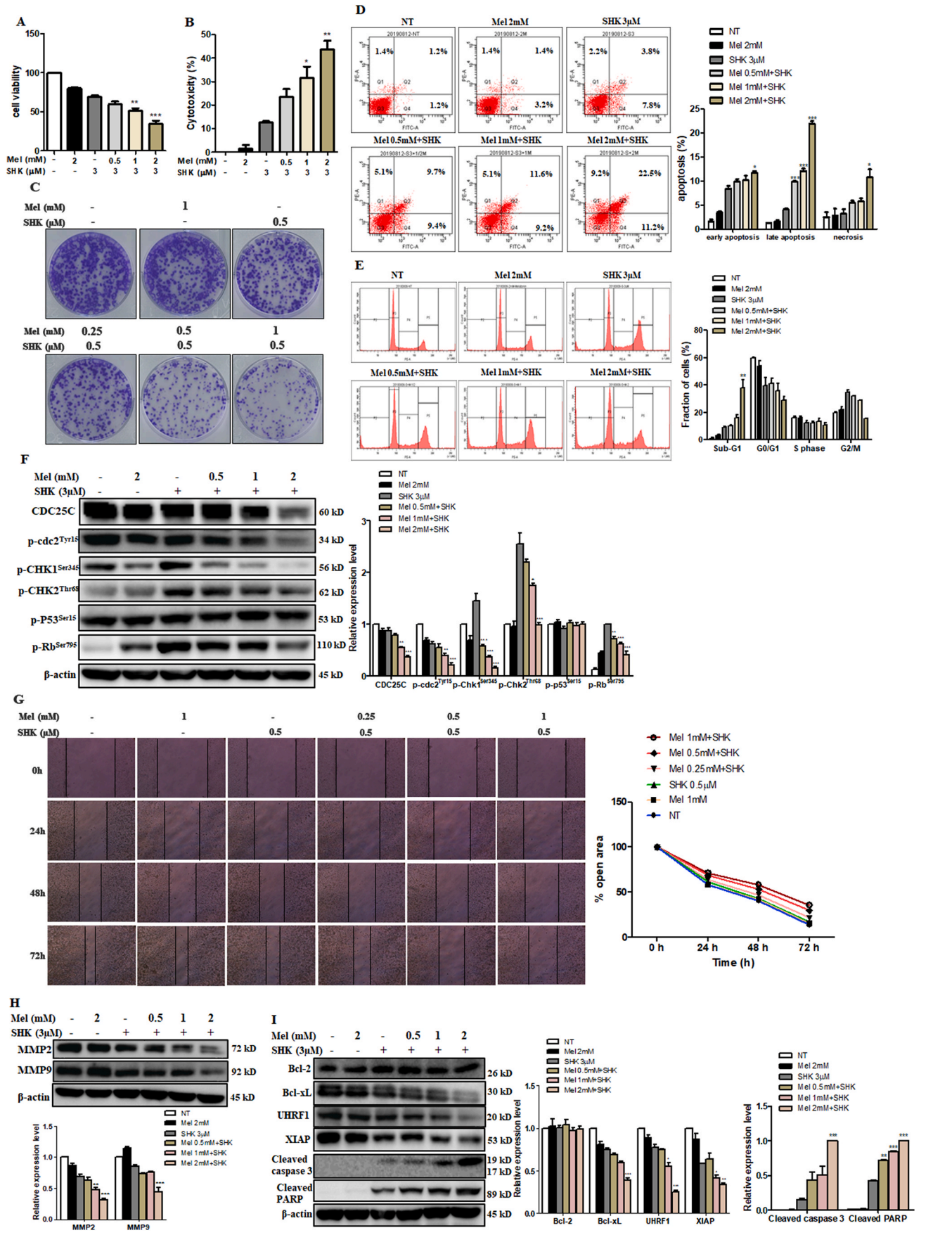

(caption on next page)

Fig. 3. Melatonin-shikonin (Mel-SHK) treatment inhibits HeLa cell growth and facilitates apoptosis. (A) Cell viability and (B) cytotoxicity were assessed in HeLa cells treated with SHK (3 μM) with or without Mel (0–2 mM). The effects of combined Mel-SHK treatment at these concentrations on (C) clonogenicity, (D) apoptosis [Annexin V/PI double-staining] and (E) sub-G1 phase accumulation were then evaluated. (F) Western blotting was used to identify the levels of several proteins associated with cell division and cell cycle. (G) A wound-healing assay was performed to investigate the effects of treatment on cell migration. The bar graph depicts the percentage of the open area remaining after treatment. Western blotting was further performed to evaluate (H) the levels of matrix metalloproteinases (MMPs) and (I) pro- and anti-apoptotic proteins in response to Mel-SHK treatment. For all experiments, the treatment duration was 24 h. Flow cytometry data are presented as histograms and bar graphs. Relative protein expression was calculated for all western blots, using actin for normalisation and as a loading control. One representative figure from at least three independent experiments is shown for each assay. The data in each bar graph are presented as the means ± SEM. *P < 0.05, **P < 0.01, and ***P < 0.001 relative to SHK treatment alone.

3.4. Mel-SHK induces ROS production and SIRT3/SOD2 pathway inhibition

Various intracellular signals, including oxidative stress, can trigger apoptosis. Mel-SHK strongly induced ROS production in HeLa cells compared with Mel or SHK alone (Fig. 4A), and this increase was associated with significant downregulation of the antioxidant proteins Gpx1, HO-1, and SOD2, as well as the deacetylase SIRT3 (Fig. 4B) [29]. Additionally, we showed that not just the expression but also the activity of SOD2 was significantly inhibited in Mel-SHK-treated HeLa cells (Fig. 4C), immunofluorescence confirmed the reduced expression of SOD2 and SIRT3 in nearly all cells subjected to combined treatment (Fig. 4D and E). In contrast, in normal cells, melatonin is known to upregulate the expression of SIRT3-SOD2 to reduce the oxidative damage [30–32]. To confirm that the responses of cancer cells to Mel treatment is the opposite of its effects in normal cells, we examined the effect of Mel treatment in normal cells (BHK, Vero, NIH3T3, and HaCaT) under oxidative stress. Our results showed that Mel treatment overcomes the toxic effects of hydrogen peroxide (H_2O_2) by increasing cell viability and decreasing ROS generation (Fig. S3), indicating the protective effects of Mel in all the normal cell types studied.

Furthermore, calcium can modulate the induction of apoptosis [33], although mitochondrial calcium was not influenced by Mel or SHK treatment, we observed a sharp increase in the number of cells with high mitochondrial free calcium after Mel-SHK treatment (Fig. 4F). Mel-SHK co-treatment also further downregulated the MMP, compared with SHK alone (Fig. 4G).

3.5. Mel-SHK induces ER stress and MAPK/Erk and AKT pathway dysregulation

As ER stress induces apoptosis and activates stress kinases [34], we explored whether Mel and SHK could lead to ER stress in HeLa cells. Mel-SHK significantly increased the expression of the ER stress markers CHOP and GRP78 after 12 h (Fig. 5A). Signalling pathways regulating apoptosis crucially require mitogen-activated protein kinases (MAPKs) such as c-Jun-*N*-terminal kinase (JNK), extracellular signal-regulated kinase (Erk), and p38. After Mel-SHK treatment, JNK and p38 phosphorylation increased significantly, while Erk phosphorylation was inhibited. The levels of total Erk, total JNK, and total p38 were unaffected (Fig. 5B). The AKT signalling pathway is a known regulator of ER stress, and the inhibition of ER stress-induced AKT signalling is important to cancer cell survival and anti-cancer treatment resistance [34–36]. The kinase PDK1 is an upstream activator of AKT, while the phosphorylation of PKCδ is a downstream target of AKT [37]. We showed that Mel-SHK treatment induced AKT and PDK1 dephosphorylation but increased PKCδ phosphorylation, without affecting the total AKT levels (Fig. 5C).

3.6. Caspase and ER stress inhibitors rescue cell death while PI3K inhibitor enhances Mel-SHK-induced cytotoxicity

Specific pathway inhibitors were used to determine the roles of MAPK and AKT signalling pathways in Mel-SHK-treated HeLa cells. Pre-treatment with Z-VAD-FMK, a pan-caspase inhibitor, neutralised Mel-SHK-induced cancer cell toxicity (Fig. 6A), reduced PARP cleavage, increased colony formation, and reduced sub-G1 phase accumulation (Fig. 6B–D). Similarly, ER-stress inhibitor (4-PBA) pre-treatment significantly reduced cytotoxicity, caspase-3 cleavage, and sub-G1 phase accumulation (Fig. 6E–G). In contrast, a JNK inhibitor (JNK–IN–8) and p38 inhibitor (SB203580) failed to exert protective effects against Mel-SHK treatment (Fig. S4A and B). Interestingly, pre-treatment with LY 294002 (PI3K/AKT inhibitor) had a further aggregative effect on cytotoxicity, colony formation, and apoptosis, as evidenced by increased PARP cleavage and sub-G1 phase accumulation (Fig. 6H–K). U0126 (MEK-1/2 inhibitor) pre-treatment had a slight but non-significant effect on cytotoxicity and anti-clonogenicity (Fig. S4C). These data suggest a downstream role for AKT signalling in Mel-SHK-induced cell death.

3.7. NAC rescues HeLa cells from the anti-cancer effects of Mel-SHK

We subsequently treated HeLa cells with NAC, a direct antioxidant and ROS scavenger [38], to confirm the Mel-SHK-induced anti-cancer effects were due to increased ROS production and oxidative stress. Pre-treatment with NAC significantly reduced the cytotoxic effects of Mel-SHK (Fig. 7A), which was confirmed by an assessment of cell morphology (Fig. S2D). Colony formation assay showed that cell death in Mel-SHK-treated HeLa cells was prevented by NAC pre-treatment, facilitating long-term survival (Fig. 7B), and the populations of both early and late apoptotic cells were significantly reduced (Fig. 7C). NAC also inhibited the Mel-SHK-induced sub-G1 phase cell accumulation, leading to an increased shift to the G0/G1 phase and upregulated CDC25C and p-cdc2 levels (Fig. 7D and S2E). Likewise, NAC further rescued the inhibitory effect of Mel-SHK on cell migration, as indicated by a substantial reduction in the open areas of a wound assay (Fig. 7E). Consistent with these findings, NAC reversed the Mel-SHK-mediated inhibition of MMP-2 and MMP-9 (Fig. 7F). Furthermore, Mel-SHK-induced cleavage of caspase-3 and PARP were completely inhibited by the pre-treatment of NAC in HeLa cells (Fig. 7G). Additionally, we showed that the protective effects of NAC against Mel-SHK were not specific to HeLa cells, as NAC pre-treatment had anti-apoptotic effects, particularly the reversal of caspase-3 and/or PARP cleavage, in MCF7, AGS, and SW480 cells (Fig. 7H–J). These effects are consistent with the inhibition of Mel-SHK-induced ROS generation by NAC (Fig. 7K).

Next, we investigated the effect of NAC pre-treatment on Mel-SHK-induced ER stress, and the MAPK and AKT pathways. In Mel-SHK-treated HeLa cells, NAC pre-treatment upregulated antioxidant proteins (Gpx1, HO-1, SOD2) and SIRT3, as well as SOD2 activity (Fig. 7L and M), and significantly reduced the numbers of cells with mitochondrial calcium overload and low MMP (Fig. 7N and O). NAC also significantly suppressed the Mel-SHK-induced expression of CHOP and GRP78 (Fig. 7P) and reduced the effects of the drug combination on Erk, p38, and JNK phosphorylation (Fig. 7Q). NAC pre-treatment further reversed the Mel-SHK-induced dephosphorylation of AKT and PDK1, while inducing the dephosphorylation of PKCδ (Fig. 7R), thus overcoming the AKT activation loop and ER stress.

3.8. The adverse effects of Mel-SHK on HeLa cells are inhibited by SIRT3

SIRT3 binds directly to SOD2 and regulates SOD2 activity [15], the

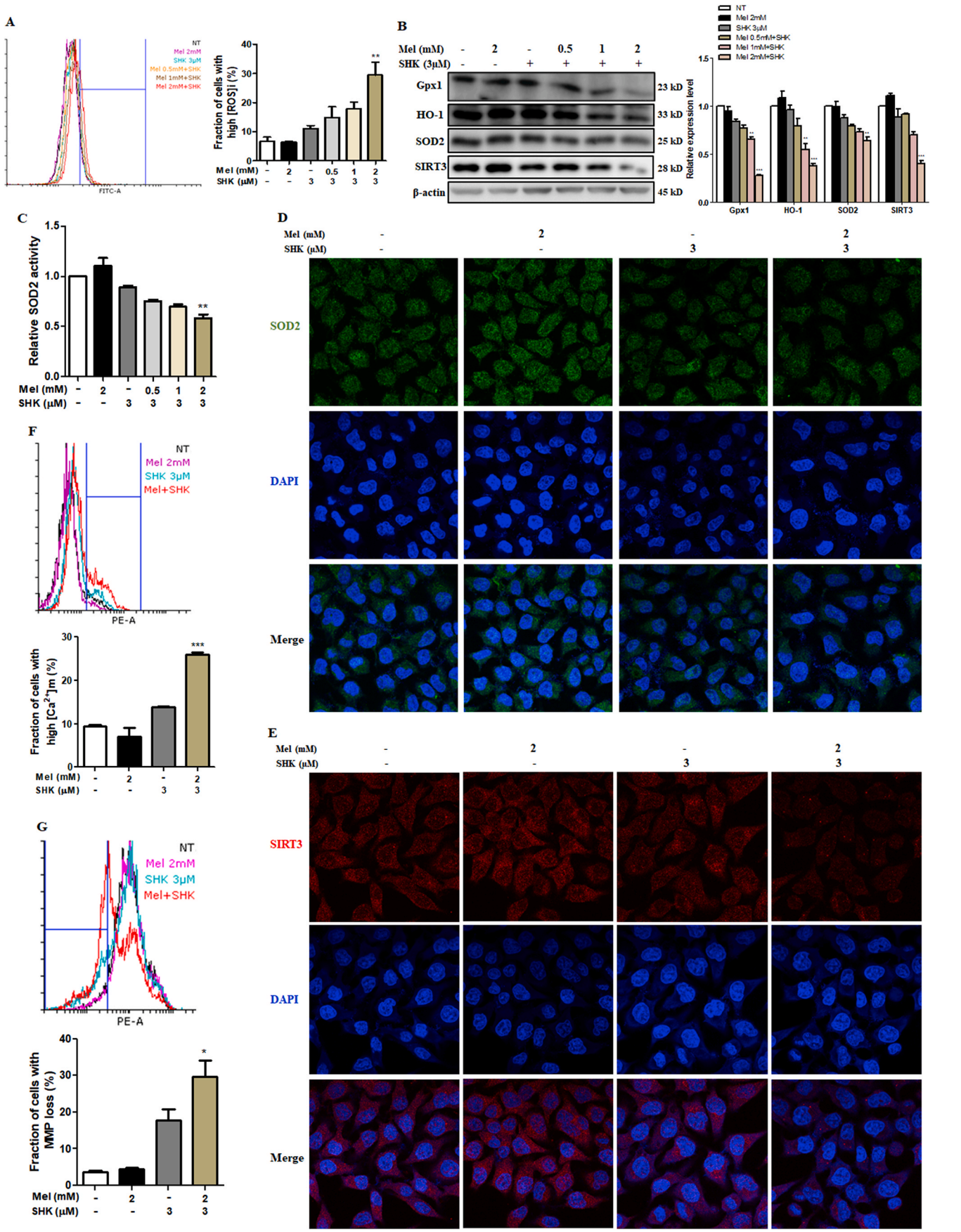

(caption on next page)

Fig. 4. Melatonin-shikonin (Mel-SHK) treatment enhances reactive oxygen species (ROS) generation and inhibits SIRT3/SOD2 pathway activation in HeLa cells. (A) The levels of ROS in HeLa cells treated with Mel-SHK for 6 h are presented as fractions of cells with high ROS. (B) The levels of key antioxidant proteins (Gpx1, HO-1, and SOD2) and SIRT3 and (C) relative SOD2 activity were measured at 12 h post-treatment. The protein expression of (D) SOD2 and (E) SIRT3 in these cells was confirmed using immunofluorescence by confocal microscopy. (F) The levels of mitochondrial free calcium (Ca^{2+}) and (G) MMP were measured in these cells at 12 h and 24 h post-Mel-SHK treatment, respectively. All experiments used SHK at 3 μM and Mel at 0–2 mM. Flow cytometry data are presented as histograms and bar graphs. Relative protein expression was calculated for all proteins in the western blots and actin was used for normalisation and as a loading control. One representative figure from at least three independent experiments is shown for each assay. The data in each bar graph are presented as the means ± SEM. *P < 0.05, **P < 0.01, and ***P < 0.001 relative to SHK treatment alone.

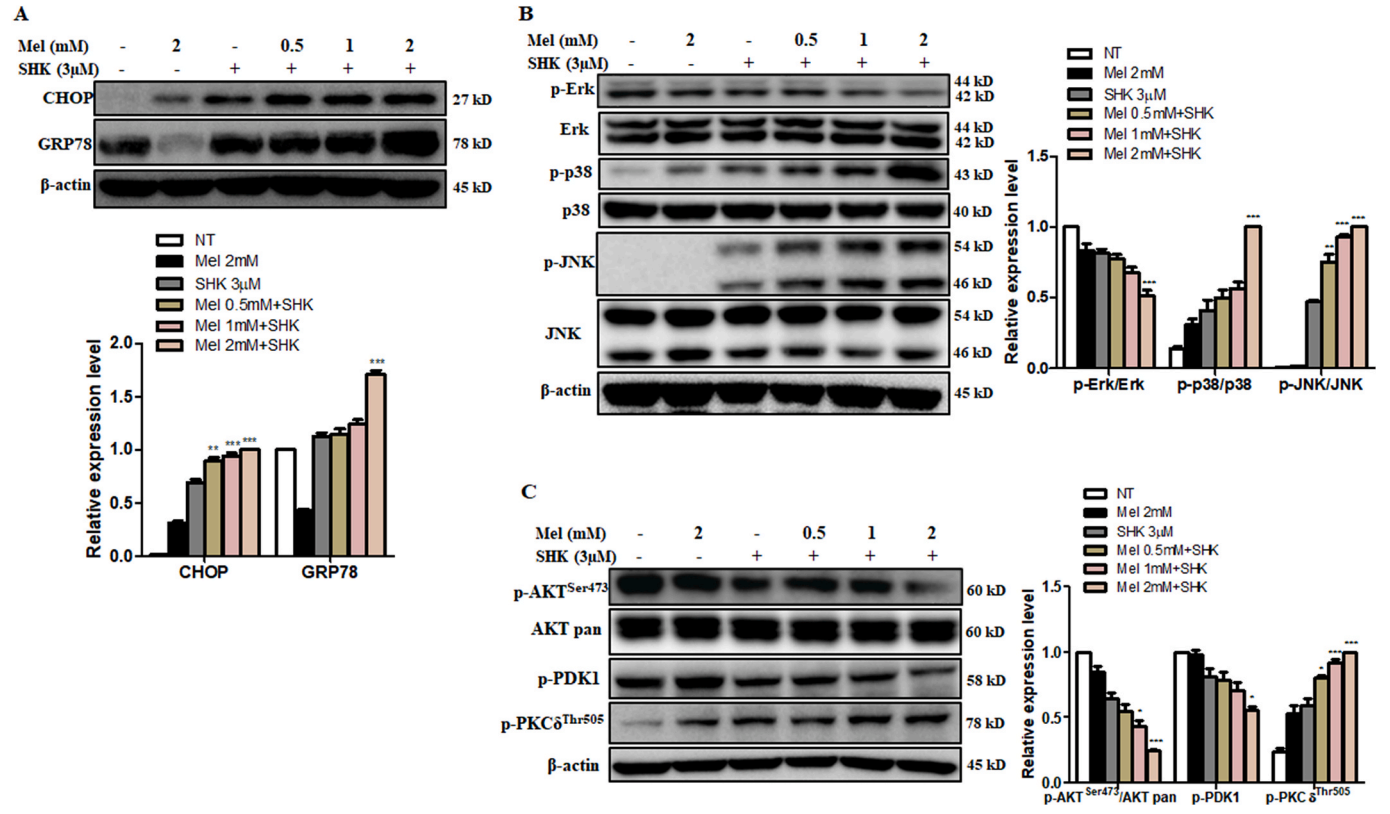

Fig. 5. Melatonin-shikonin (Mel-SHK) treatment enhances endoplasmic reticulum (ER) stress and MAPK and AKT pathway dysregulation in HeLa cells. (A) Western blot analysis of the specific ER stress-related proteins, CHOP and GRP78 and (B) the levels and activation (i.e., phosphorylation) of ERK, p38, and JNK. (C) Quantitative Western blot analysis to determine the activation of the AKT pathway components p-AKT, p-PDK1, and p-PKC, as well as total AKT. Relative protein expression was calculated for all proteins in the western blots. Actin was used for normalisation and as a loading control. One representative figure from at least three independent experiments is shown for each assay. The data in each bar graph are presented as the means ± SEM. *P < 0.05, **P < 0.01, and ***P < 0.001 relative to SHK treatment alone.

immunoprecipitation of SOD2 revealed a dramatic decrease in SIRT3–SOD2 binding in cells treated with Mel-SHK, but not with individual drug (Fig. 8A). To determine the role of SIRT3 in Mel-SHK-induced cell death, HeLa cells were pre-treated with 4-BR, a broad-spectrum SIRT inhibitor. Although 50 μM 4-BR treatment alone had no effect, subsequent Mel-SHK treatment led to further increases in caspase-3 cleavage, sub-G1 phase accumulation and MMP losses, compared to Mel-SHK treatment (Fig. 8B–D).

To further confirm the role of decreased SIRT3-SOD2 expression in Mel-SHK-induced cancer cell death, HeLa cells were transfected with SIRT3-expressing plasmids (Fig. 8E). In response to Mel-SHK, these SIRT3-overexpressing cells exhibited a significant reduction in sub-G1 cell accumulation, as well as reduced PARP cleavage and ROS generation, concomitant with increased SOD2 expression (Fig. 8F–I). In addition, SIRT3 overexpression significantly reduced the fractions of cells with mitochondrial free calcium and a low MMP induced by Mel-SHK treatment (Fig. 8J and K). Moreover, SIRT3 overexpression also inhibited the expression of CHOP and GRP78 (Fig. 8L) and reversed the levels of proteins associated with MAPK and AKT signalling pathways in Mel-SHK-treated HeLa cells (Fig. 8M and N). These results suggest that SIRT3 inhibition is the key factor in the effects of Mel-SHK on oxidative stress, ER stress, apoptosis, and cell growth via SIRT3/SOD2 and AKT pathway inhibition.

4. Discussion

In recent studies, cancers that were initially resistant to chemotherapy became sensitive when conventional drugs were combined with Mel [39,40]. However, few studies identified a common target molecule. In this study, we demonstrated for the first time that Mel sensitised SHK-induced cancer cell cytotoxicity by inhibiting SIRT3/SOD2 expression and SOD2 activity. Mel-SHK treatment promoted apoptosis and induced ER stress, leading to AKT inactivation via increased ROS production in various cancer cell types (Fig. 9), suggesting the broad chemotherapeutic potential of the Mel-SHK combination and the SIRT3/SOD2-AKT pathway as a novel drug target.

SOD2, an antioxidant enzyme and important regulator of mitochondrial redox balance, is deacetylated by SIRT3, leading to enhanced antioxidant activity and decreased ROS generation [41]. Previously, SIRT3 downregulation, decreased SOD2 activity, and increased ROS

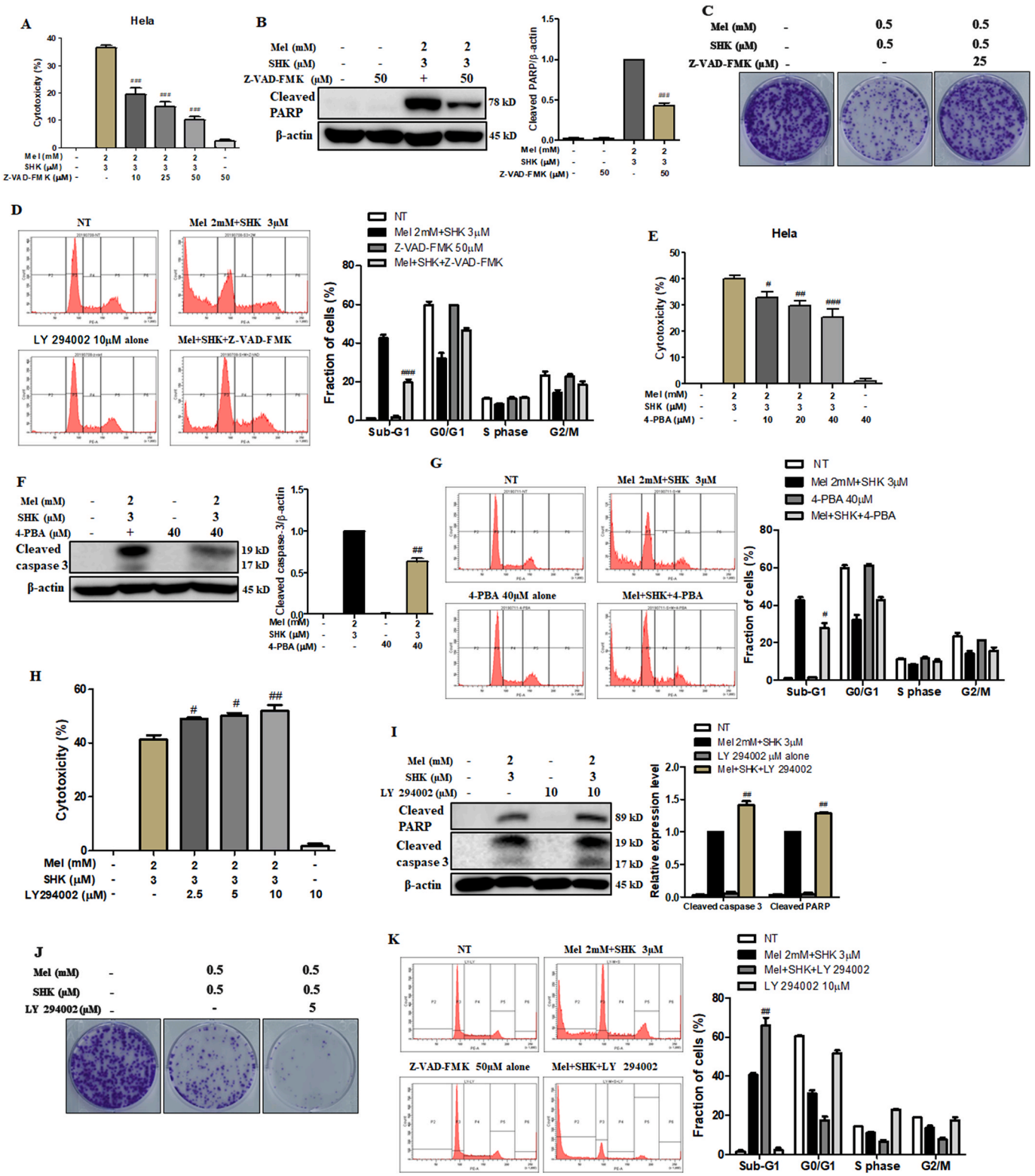

Fig. 6. Effects of a pan-caspase inhibitor (Z-VAD-FMK), endoplasmic reticulum (ER) stress inhibitor (4-PBA) and PI3K inhibitor (LY 294002) in melatonin-shikonin (Mel-SHK)-treated HeLa cells. (A) Cytotoxicity, (B) PARP cleavage, (C) clonogenicity, and (D) sub-G1 phase accumulation were determined after pre-treatment with Z-VAD-FMK. (E) Cytotoxicity, (F) caspase-3 cleavage, and (G) sub-G1 phase accumulation were also determined in cells pre-treated with 4-PBA. (H) Cytotoxicity, (I) PARP cleavage, (G) clonogenicity, and (K) sub-G1 phase accumulation were determined in cells pre-treated with LY 294002 to determine the involvement of the AKT pathway in Mel-SHK-induced cancer cells. Flow cytometry data are presented as histograms and bar graphs. Relative protein expression was calculated for all the proteins in western blots. Actin was used for normalisation and as a loading control. One representative figure from at least three independent experiments is shown for each assay. The data in each bar graph are presented as the means ± SEM. $^{\#}P < 0.05$, $^{\#\#}P < 0.01$, and $^{\#\#\#}$, $P < 0.001$ relative to Mel-SHK treated cells.

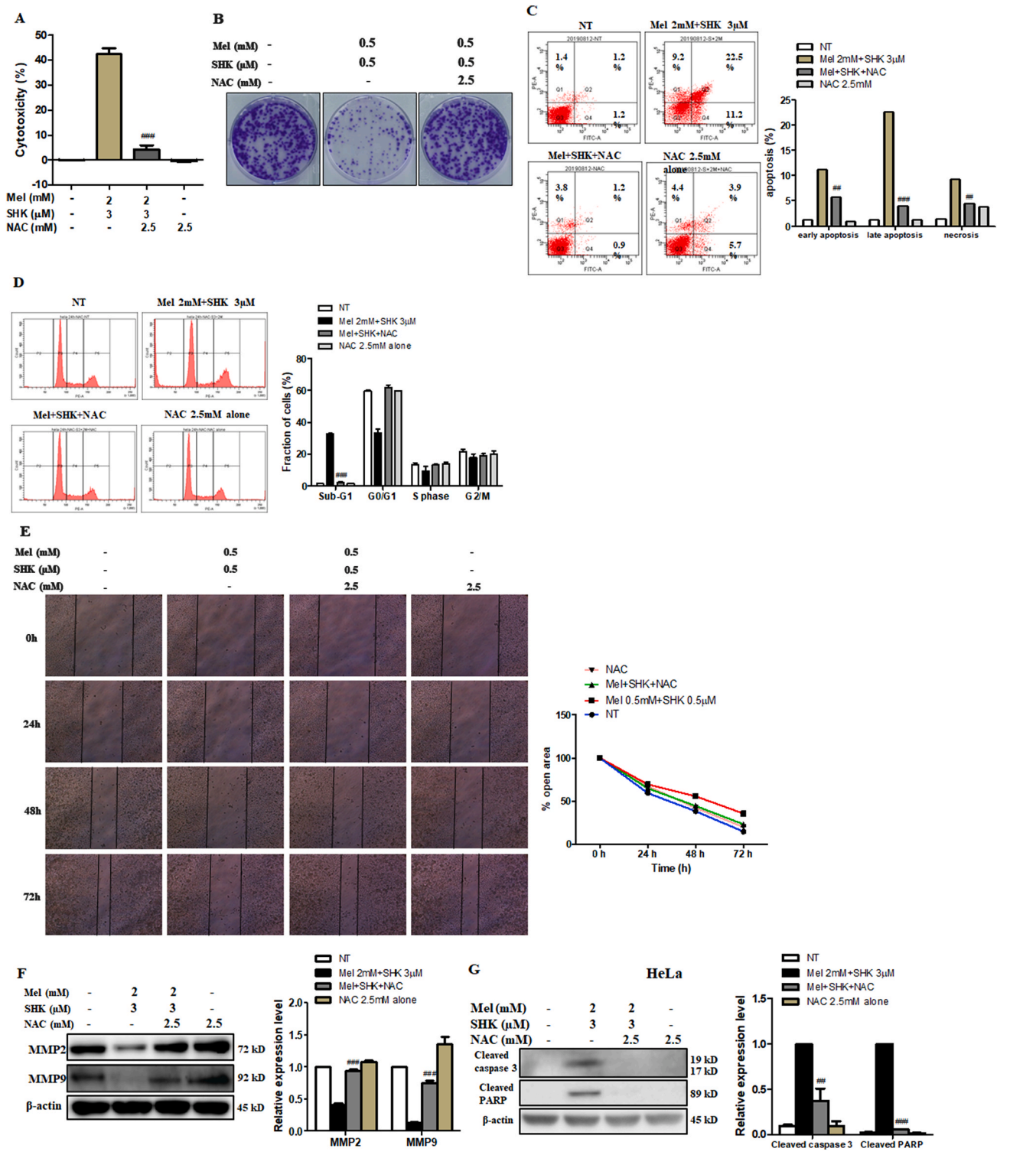

Fig. 7. Effects of the reactive oxygen species (ROS) scavenger, NAC, on the anti-cancer effects of melatonin-shikonin (Mel-SHK) in HeLa, MCF7, AGS, and SW480 cells. HeLa cells were pre-treated with NAC followed by Mel-SHK. The effects on (A) cytotoxicity, (B) clonogenicity, (C) apoptosis [Annexin V/PI double-staining], (D) sub-G1 area, and (E) cell migration were evaluated to confirm the role of ROS. (F) Western blotting was performed to analyse the levels of specific proteins related to cell migration, such as matrix metalloproteinase-2 (MMP2) and MMP9. The protective effects of NAC against Mel-SHK-induced apoptosis including caspase-3 and/or PARP cleavage, were determined in (G) HeLa, (H) MCF7, (I) AGS and (J) SW480 cells. The ability of NAC to reverse Mel-SHK-mediated (K) ROS generation, (L) oxidative stress-related protein expression, (M) SOD2 activation, (N) mitochondrial calcium (Ca^{2+}) accumulation, (O) MMP losses and (P) ER-stress related protein expression were also investigated. (Q, R) Western blot analysis of the effects of NAC on the expression of MAPK and AKT pathway-related proteins in Mel-SHK-treated cells. The Mel-SHK treatment duration was 24 h for all experiments except those described in B (10 days), K (6 h) and L, M, N, P, Q and R (12 h). Relative protein expression was calculated for all the proteins in western blots. Actin was used for normalisation and as a loading control. Flow cytometry data are presented as histograms and bar graphs. One representative figure from at least three independent experiments is shown for each assay. The data in each bar graph are presented as the means ± SEM. $^{\#}P < 0.05$, $^{\#\#}P < 0.01$, and $^{\#\#\#}P < 0.001$ relative to Mel-SHK treated cells.

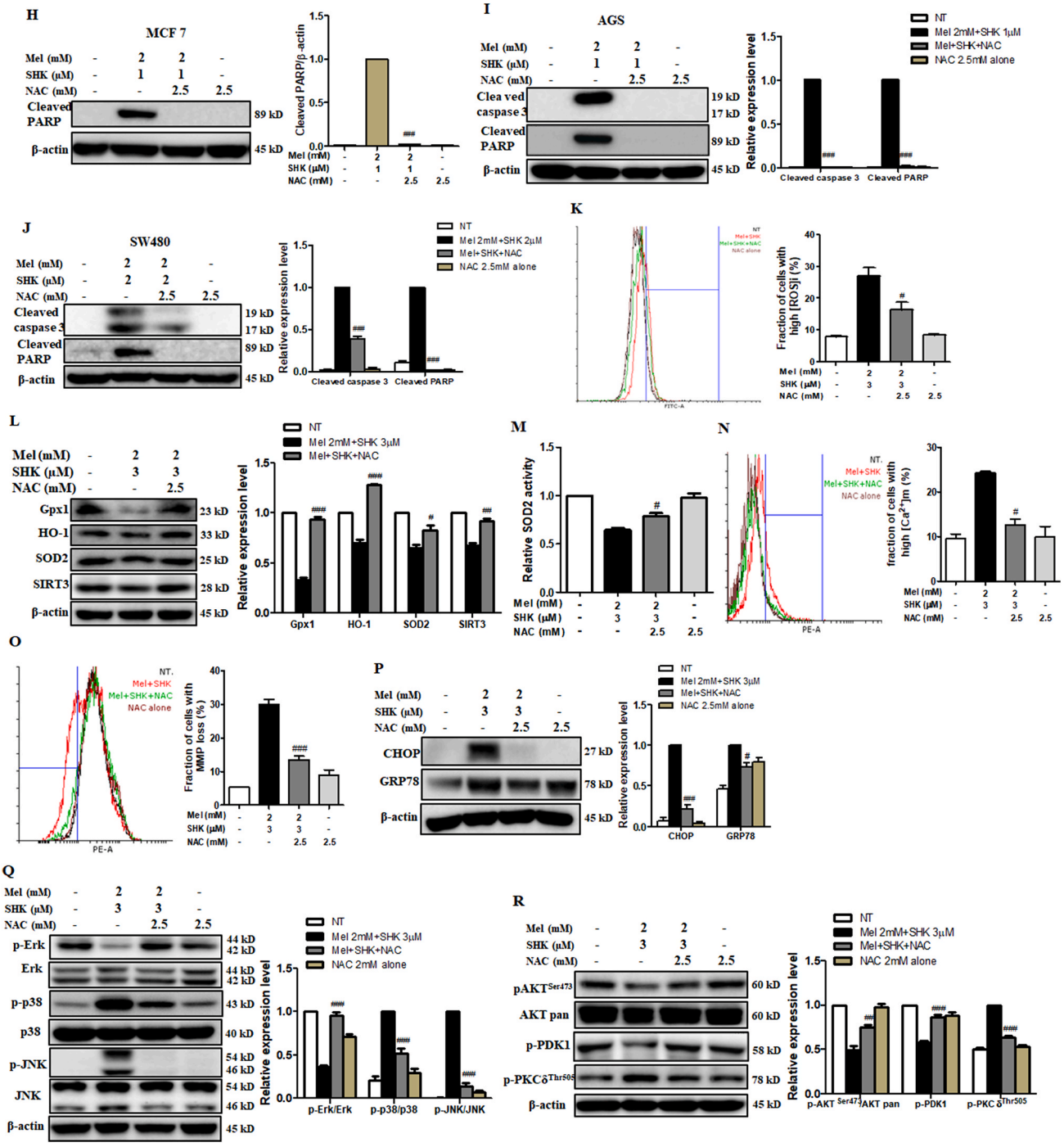

Fig. 7. (*continued*).

production were found to contribute to the anti-tumour effects of linalool against glioma [42]. Similarly, we showed that Mel-SHK inhibited SOD2 activity and increased the fraction of cells with high ROS levels, which led to increases in mitochondrial calcium levels, MMP disruption, and apoptosis in various cancer cells. All these effects were reversed by treatment with a ROS scavenger, suggesting that excessive oxidative stress plays a key role in Mel-SHK-induced cytotoxicity in cancer cells. Several studies have reported that Mel treatment induces cell death in cancer cells but has beneficial effects on normal cells [30–32,43,44]. This is probably because Mel induces the release of mitochondrial cytochrome C, leading to apoptosis in cancer cells [45]. Also, Mel treatment in cancer cells is known to interact with mitochondrial ROS forming a range of metabolites such as *N*-acetylserotonin, which can induce apoptosis. However, this phenomenon does not occur in normal cells [3]. Hence, the difference in Mel metabolism between normal and tumour cells is beneficial to the chemotherapy, which causes severe side effects to normal cells. In this study, we also showed that Mel potentiated the efficiency of SHK-induced cancer cell cytotoxicity and, at the same time, protected normal cells from oxidative stress.

Tumour cells characteristically exhibit a loss of control of the balance between proliferation and death. Interventional cancer therapies aim to steer this balance towards the induction of apoptotic cell death, a process prevented by Bcl-2 and Bcl-xL but promoted by Bak and Bax, which activate pro-apoptotic signals, and caspase activation and cleavage [46]. In a previous report, SHK stimulated apoptosis in squamous cell carcinoma cells by downregulating Bcl-2, upregulating Bax, and inducing

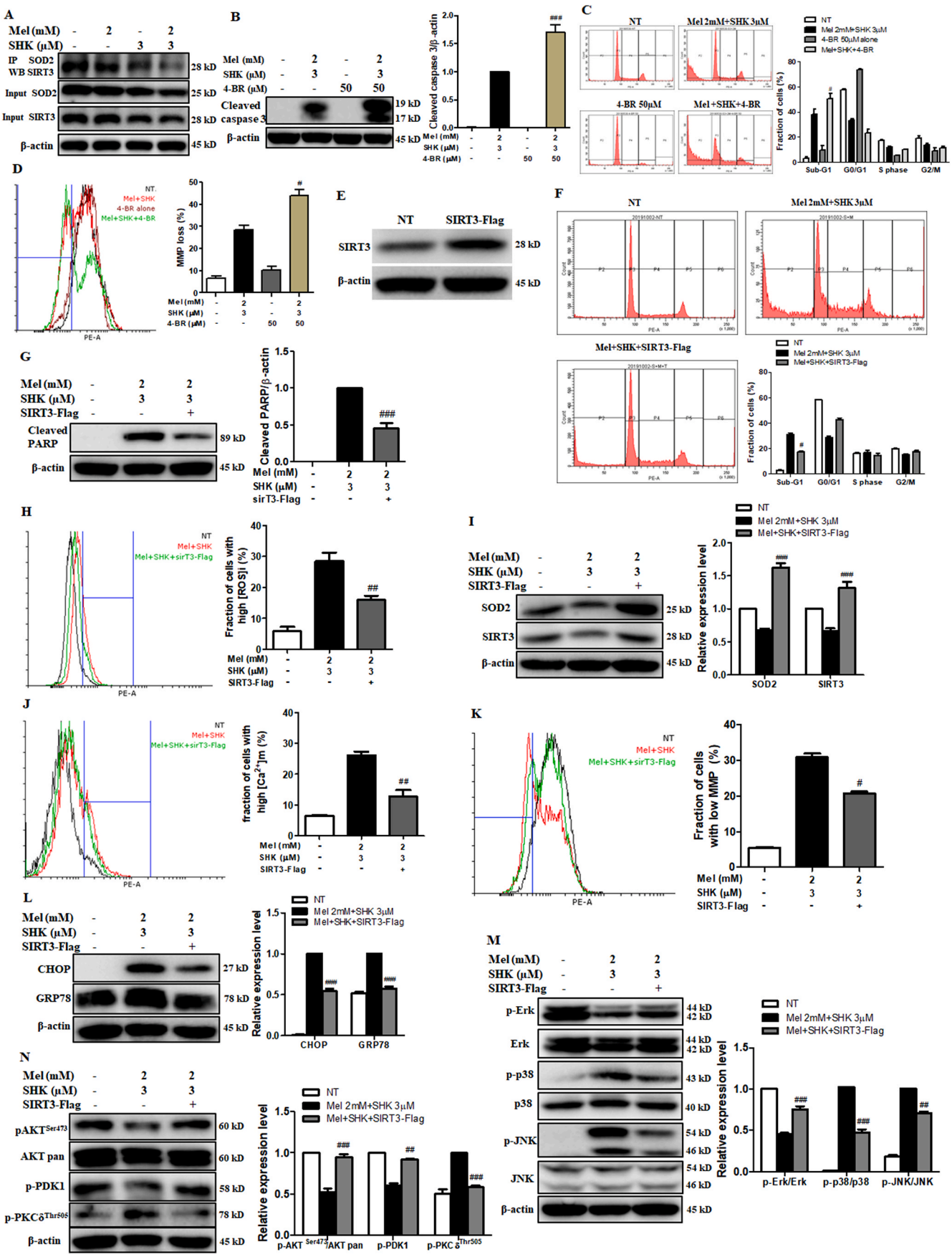

(caption on next page)

Fig. 8. Effects of SIRT inhibition and SIRT3 overexpression on the melatonin-shikonin (Mel-SHK)-induced HeLa cell cytotoxicity. (A) Immunoprecipitation analysis to demonstrate the effects of Mel and/or SHK on the direct binding of SIRT3 with SOD2. (B) apoptosis via caspase activation, (C) sub-G1 phase accumulation and (D) MMP losses were investigated in HeLa cells pre-treated with the SIRT inhibitor 4-BR before combined treatment with Mel-SHK to examine the role of SIRT3/SOD2 in Mel-SHK-induced cancer cell death. (E) SIRT3 overexpression in HeLa cells transfected with sirT3-Flag plasmid was confirmed by western blotting. (F–L) SIRT3-overexpressing HeLa cells were treated with Mel-SHK, and all parameters previously shown to be affected by Mel-SHK were evaluated. (M, N) The effect of SIRT3 overexpression on the MAPK and AKT pathways was also evaluated. Relative protein expression was calculated for all the proteins in western blots. Actin was used for normalisation and as a loading control. All experiments used SHK at 3 μM and Mel at 0–2 mM. Flow cytometry data are presented as histograms and bar graphs. One representative figure from at least three independent experiments is shown for each assay. The data in each bar graph are presented as the means ± SEM. $^{\#}P < 0.05$, $^{\#\#}P < 0.01$, and $^{\#\#\#}P < 0.001$ relative to Mel-SHK treated cells.

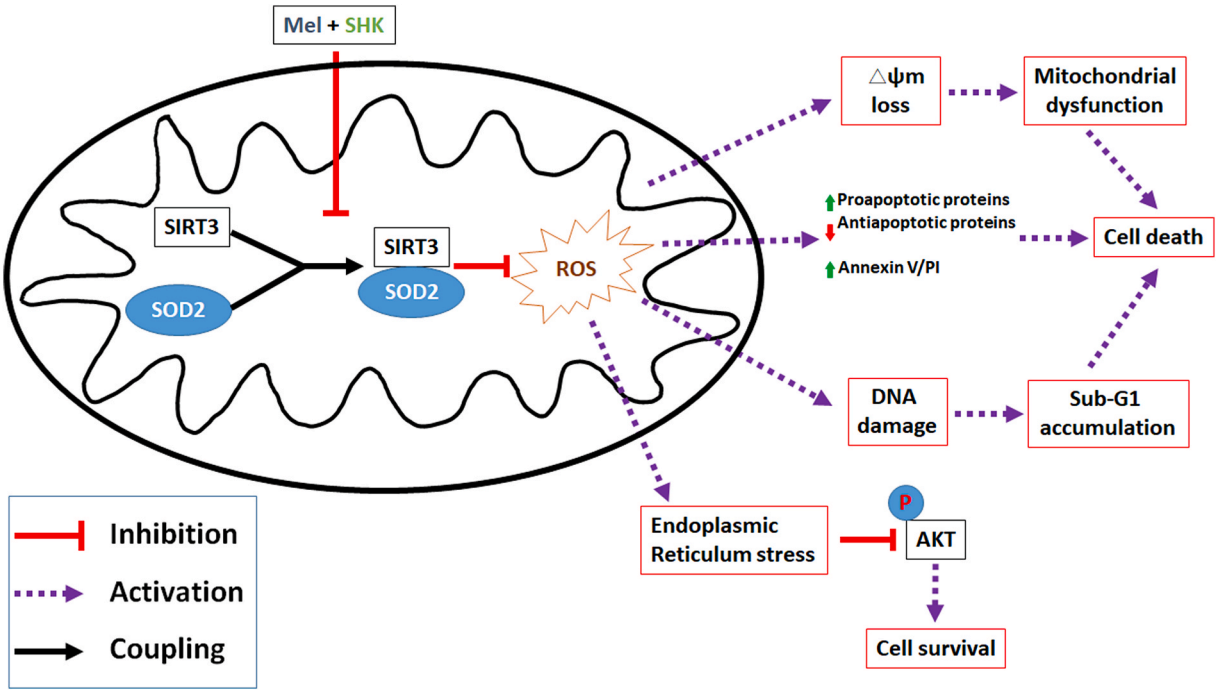

Fig. 9. Schematic illustration showing the mechanism of melatonin (Mel) sensitises shikonin (SHK)-induced cancer cell death.

caspase-3 cleavage [47]. Similarly, Cucina et al. reported that Mel-induced apoptosis activated caspases, cleaved PARP, and concomitantly decreased the Bcl-2/Bax ratio in breast cancer cells [48]. Consistent with those findings, we demonstrated that Mel-SHK combination therapy had significant pro-apoptotic effects in HeLa cells, which was counteracted by a pan-caspase inhibitor.

Lin et al. recently reported that a combination of Mel and sorafenib inhibited hepatocellular carcinoma cell growth and apoptosis via the JNK pathway in a dose-dependent manner [49]. When used co-operatively, Mel and SHK exert an enhanced anticancer effect mediated by apoptotic cell death in various cancer cells in correlation with caspase 3 activation, PARP cleavage, and JNK pathway activation. However, a JNK inhibitor did not block the apoptosis induced by Mel-SHK. As the JNK pathway is activated by high ROS levels [50], we believe that the JNK inhibitor was not strong enough to overcome the effects of ROS-mediated JNK pathway activation induced by Mel-SHK. The combination of Mel-SHK might enhance cancer cell death by regulating oxidative stress. We also evaluated the potential involvement of other types of pathways, such as necroptosis, in Mel-SHK-induced cell death by incubating HeLa cells with the novel and highly active necroptosis inhibitors Necrostatin-1 (Nec-1, a specific inhibitor of RIP1 kinase) and necrosulfonamide (NSA, a specific inhibitor of necrosis downstream of RIP3 activation). Nec-1 pre-treatment appeared to inhibit cytotoxicity and restored colony formation in Mel-SHK-treated cells, whereas NSA pre-treatment had no such protective effects (Fig. S4D and E). Accordingly, we are currently exploring the potential involvement of necroptosis and RIP1, but not RIP3, as a key factor in Mel-SHK-induced cell death.

Evidences suggest that ER stress inhibition favours cancer cell survival and enhances chemotherapeutic resistance [51,52]. Prolonged and severe ER stress can have a cytotoxic effect by activating mechanisms involved in apoptotic cell death. Mel, when combined with several other chemotherapeutic drugs, has shown its utility in cancer treatment by modulating ER stress via the Erk/MAPK and AKT pathways [53]. Furthermore, in colon cancer, SHK-induced cell death appears to be mediated by ER stress activation via MAPK signalling [54,55]. Here, we demonstrated that the combination of Mel and SHK strongly induced ER stress and cancer cell death, possibly by regulating the MAPK and AKT pathways in these cells. Moreover, pre-treatment with an ER stress inhibitor reduced the cytotoxicity associated with Mel-SHK treatment in HeLa cells, whereas PI3K/AKT inhibitor treatment further intensified the cytotoxicity and sub-G1 phase accumulation.

In conclusion, our results suggested that the onco-static and cytotoxic effects of Mel-SHK combination therapy are likely due to SIRT3/SOD2-AKT pathway inhibition. We further suggest that SIRT3-SOD2 acts as a master regulator of key cellular processes required for cancer cell survival. Thus, the Mel-SHK-induced inhibition of these molecules may represent a novel chemotherapeutic approach. We recommend the consideration of this powerful drug combination as a potential chemotherapeutic candidate for *in vivo* studies and as an adjuvant therapy in clinical trials.

Author contributions

Mengling Li designed and performed the experiments, analysed data, prepared the figures, and drafted the manuscript. Jibran Sualeh

Muhammad provided intellectual input, prepared schematic illustration figure, drafted, and edited the manuscript. Chengai Wu and Dan Yan analysed part of the data and prepared the figures. Koichi Tsuneyama and Hideki Hatta provided some technical guidance for experiments. Zheng-Guo Cui and Hidekuni Inadera contributed to this work by designing experiments, providing intellectual input, supervising the research, and edited the manuscript. All authors reviewed and approved the final manuscript for submission.

Declaration of competing interest

The authors declare no conflict of interest.

Acknowledgements

This study was supported by JSPS KAKENHI Grant No. 17K09154, 18K10044 and 20K10449. We would like to thank the other members in our team (Shahbaz Ahmad Zakki, Qianwen Feng, Lu Sun, Yulin Li) and Prof. Takashi Kondo (Department of Radiological Sciences, Graduate School of Medicine and Pharmaceutical Sciences, University of Toyama, Japan) for their generous help in the experimental studies.

Appendix A. Supplementary data

Supplementary data to this article can be found online at https://doi.org/10.1016/j.redox.2020.101632.

References

[1] F. Bray, J. Ferlay, I. Soerjomataram, R.L. Siegel, L.A. Torre, A. Jemal, Global cancer statistics 2018: GLOBOCAN estimates of incidence and mortality worldwide for 36 cancers in 185 countries, Ca - Cancer J. Clin. 68 (6) (2018) 394–424.

[2] L.R. Zarour, S. Anand, K.G. Billingsley, W.H. Bisson, A. Cercek, M.F. Clarke, L. M. Coussens, C.E. Gast, C.B. Geltzeiler, L. Hansen, K.A. Kelley, C.D. Lopez, S. R. Rana, R. Ruhl, V.L. Tsikitis, G.M. Vaccaro, M.H. Wong, S.C. Mayo, Colorectal cancer liver metastasis: evolving paradigms and future directions, Cell Mol. Gastroenterol. Hepatol. 3 (2) (2017) 163–173.

[3] R.J. Reiter, D.X. Tan, Mitochondria: the birth place, battle ground and the site of melatonin metabolism in cells, Melatonin Res. 2 (1) (2019) 44–66.

[4] C. Savvidis, M. Koutsilieris, Circadian rhythm disruption in cancer biology, Mol. Med. 18 (2012) 1249–1260.

[5] K. Mortezaee, M. Najafi, B. Farhood, A. Ahmadi, Y. Potes, D. Shabeeb, A.E. Musa, Modulation of apoptosis by melatonin for improving cancer treatment efficiency: an updated review, Life Sci. 228 (2019) 228–241.

[6] C. Guo, J. He, X. Song, L. Tan, M. Wang, P. Jiang, Y. Li, Z. Cao, C. Peng, Pharmacological properties and derivatives of shikonin-A review in recent years, Pharmacol. Res. 149 (2019) 104463.

[7] W. Liang, J. Cui, K. Zhang, H. Xi, A. Cai, J. Li, Y. Gao, C. Hu, Y. Liu, Y. Lu, N. Wang, X. Wu, B. Wei, L. Chen, Shikonin induces ROS-based mitochondria-mediated apoptosis in colon cancer, Oncotarget 8 (65) (2017) 109094–109106.

[8] Y. Liu, X. Kang, G. Niu, S. He, T. Zhang, Y. Bai, Y. Li, H. Hao, C. Chen, Z. Shou, B. Li, Shikonin induces apoptosis and prosurvival autophagy in human melanoma A375 cells via ROS-mediated ER stress and p38 pathways, Artif Cells Nanomed. Biotechnol. 47 (1) (2019) 626–635.

[9] B. Wiench, T. Eichhorn, M. Paulsen, T. Efferth, Shikonin directly targets mitochondria and causes mitochondrial dysfunction in cancer cells, Evid Based Compl. Altern. Med. 2012 (2012) 726025.

[10] J.H. Jung, E.J. Sohn, E.A. Shin, D. Lee, B. Kim, D.B. Jung, J.H. Kim, M. Yun, H. J. Lee, Y.K. Park, S.H. Kim, Melatonin suppresses the expression of 45S preribosomal RNA and upstream binding factor and enhances the antitumor activity of puromycin in MDA-MB-231 breast cancer cells, Evid Based Compl. Altern. Med. 2013 (2013) 879746.

[11] P.A. Kosar, M. Naziroglu, I.S. Ovey, B. Cig, Synergic effects of doxorubicin and melatonin on apoptosis and mitochondrial oxidative stress in MCF-7 breast cancer cells: involvement of TRPV1 channels, J. Membr. Biol. 249 (1–2) (2016) 129–140.

[12] M. Margheri, N. Pacini, A. Tani, D. Nosi, R. Squecco, A. Dama, E. Masala, F. Francini, S. Zecchi-Orlandini, L. Formigli, Combined effects of melatonin and all-trans retinoic acid and somatostatin on breast cancer cell proliferation and death: molecular basis for the anticancer effect of these molecules, Eur. J. Pharmacol. 681 (1–3) (2012) 34–43.

[13] H.J. Weir, J.D. Lane, N. Balthasar, SIRT3: a central regulator of mitochondrial adaptation in Health and disease, Genes Canc. 4 (3–4) (2013) 118–124.

[14] W.C. Hallows, S. Lee, J.M. Denu, Sirtuins deacetylate and activate mammalian acetyl-CoA synthetases, Proc. Natl. Acad. Sci. U. S. A. 103 (27) (2006) 10230–10235.

[15] Y.S. Kim, P. Gupta Vallur, R. Phaeton, K. Mythreye, N. Hempel, Insights into the dichotomous regulation of SOD2 in cancer, Antioxidants 6 (4) (2017) 86.

[16] J. Lu, K. Cheng, B. Zhang, H. Xu, Y. Cao, F. Guo, X. Feng, Q. Xia, Novel mechanisms for superoxide-scavenging activity of human manganese superoxide dismutase determined by the K68 key acetylation site, Free Radic. Biol. Med. 85 (2015) 114–126.

[17] S.J. Allison, J. Milner, SIRT3 is pro-apoptotic and participates in distinct basal apoptotic pathways, Cell Cycle 6 (21) (2007) 2669–2677.

[18] J. Kong, L. Wang, L. Ren, Y. Yan, Y. Cheng, Z. Huang, F. Shen, Triptolide induces mitochondria-mediated apoptosis of Burkitt's lymphoma cell via deacetylation of GSK-3beta by increased SIRT3 expression, Toxicol. Appl. Pharmacol. 342 (2018) 1–13.

[19] F. Wu, W.J. Chen, L. Yan, G.Q. Tan, W.T. Li, X.J. Zhu, X.C. Ge, J.W. Liu, B.L. Wang, Mus81 knockdown improves chemosensitivity of hepatocellular carcinoma cells by inducing S-phase arrest and promoting apoptosis through CHK1 pathway, Canc. Med. 5 (2) (2016) 370–385.

[20] S.M. Smith, M.B. Wunder, D.A. Norris, Y.G. Shellman, A simple protocol for using a LDH-based cytotoxicity assay to assess the effects of death and growth inhibition at the same time, PloS One 6 (11) (2011), e26908.

[21] T.C. Chou, Drug combination studies and their synergy quantification using the Chou-Talalay method, Canc. Res. 70 (2) (2010) 440–446.

[22] T.C. Chou, P. Talalay, Quantitative analysis of dose-effect relationships: the combined effects of multiple drugs or enzyme inhibitors, Adv. Enzym. Regul. 22 (1984) 27–55.

[23] D.P. Li, Y.L. Chen, H.Y. Jiang, Y. Chen, X.Q. Zeng, L.L. Xu, Y. Ye, C.Q. Ke, G. Lin, J. Y. Wang, H. Gao, Phosphocreatine attenuates Gynura segetum-induced hepatocyte apoptosis via a SIRT3-SOD2-mitochondrial reactive oxygen species pathway, Drug Des. Dev. Ther. 13 (2019) 2081–2096.

[24] C. Wang, R.J. Youle, The role of mitochondria in apoptosis, Annu. Rev. Genet. 43 (2009) 95–118.

[25] R. Rahbari, T. Sheahan, V. Modes, P. Collier, C. Macfarlane, R.M. Badge, A novel L1 retrotransposon marker for HeLa cell line identification, Biotechniques 46 (4) (2009) 277–284.

[26] S.V. Singh, A. Herman-Antosiewicz, A.V. Singh, K.L. Lew, S.K. Srivastava, R. Kamath, K.D. Brown, L. Zhang, R. Baskaran, Sulforaphane-induced G2/M phase cell cycle arrest involves checkpoint kinase 2-mediated phosphorylation of cell division cycle 25C, J. Biol. Chem. 279 (24) (2004) 25813–25822.

[27] C. Walker, E. Mojares, A. Del Rio Hernandez, Role of extracellular matrix in development and cancer progression, Int. J. Mol. Sci. 19 (10) (2018) 3028.

[28] H. Zhang, H. Liu, Y. Chen, X. Yang, P. Wang, T. Liu, M. Deng, B. Qin, C. Correia, S. Lee, J. Kim, M. Sparks, A.A. Nair, D.L. Evans, K.R. Kalari, P. Zhang, L. Wang, Z. You, S.H. Kaufmann, Z. Lou, H. Pei, A cell cycle-dependent BRCA1-UHRF1 cascade regulates DNA double-strand break repair pathway choice, Nat. Commun. 7 (2016) 10201.

[29] J. He, X. Liu, C. Su, F. Wu, J. Sun, J. Zhang, X. Yang, C. Zhang, Z. Zhou, X. Zhang, X. Lin, J. Tao, Inhibition of mitochondrial oxidative damage improves reendothelialization capacity of endothelial progenitor cells via SIRT3 (sirtuin 3)-enhanced SOD2 (superoxide dismutase 2) deacetylation in hypertension, Arterioscler. Thromb. Vasc. Biol. 39 (8) (2019) 1682–1698.

[30] L. Han, H. Wang, L. Li, X. Li, J. Ge, R.J. Reiter, Q. Wang, Melatonin protects against maternal obesity-associated oxidative stress and meiotic defects in oocytes via the SIRT3-SOD2-dependent pathway, J. Pineal Res. 63 (3) (2017), e12431.

[31] W. Zhou, Y. Liu, J. Shen, B. Yu, J. Bai, J. Lin, X. Guo, H. Sun, Z. Chen, H. Yang, Y. Xu, D. Geng, Melatonin increases bone mass around the prostheses of OVX rats by ameliorating mitochondrial oxidative stress via the SIRT3/SOD2 signaling pathway, Oxid Med. Cell Longev. (2019) 4019619, 2019.

[32] Y. Chen, W. Qing, M. Sun, L. Lv, D. Guo, Y. Jiang, Melatonin protects hepatocytes against bile acid-induced mitochondrial oxidative stress via the AMPK-SIRT3-SOD2 pathway, Free Radic. Res. 49 (10) (2015) 1275–1284.

[33] W.T. Chiu, H.A. Chang, Y.H. Lin, Y.S. Lin, H.T. Chang, H.H. Lin, S.C. Huang, M. J. Tang, M.R. Shen, Bcl(-)2 regulates store-operated Ca(2+) entry to modulate ER stress-induced apoptosis, Cell Death Disc. 4 (2018) 37.

[34] A.M. Gorman, S.J. Healy, R. Jager, A. Samali, Stress management at the ER: regulators of ER stress-induced apoptosis, Pharmacol. Ther. 134 (3) (2012) 306–316.

[35] J. Tan, X. Jiang, G. Yin, L. He, J. Liu, Z. Long, Z. Jiang, K. Yao, Anacardic acid induces cell apoptosis of prostatic cancer through autophagy by ER stress/DAPK3/Akt signaling pathway, Oncol. Rep. 38 (3) (2017) 1373–1382.

[36] C. Appenzeller-Herzog, M.N. Hall, Bidirectional crosstalk between endoplasmic reticulum stress and mTOR signaling, Trends Cell Biol. 22 (5) (2012) 274–282.

[37] H.W. Yung, D.S. Charnock-Jones, G.J. Burton, Regulation of AKT phosphorylation at Ser473 and Thr308 by endoplasmic reticulum stress modulates substrate specificity in a severity dependent manner, PloS One 6 (3) (2011), e17894.

[38] I. Elbini Dhouib, M. Jallouli, A. Annabi, N. Gharbi, S. Elfazaa, M.M. Lasram, A minireview on N-acetylcysteine: an old drug with new approaches, Life Sci. 151 (2016) 359–363.

[39] R.J. Reiter, S.A. Rosales-Corral, D.X. Tan, D. Acuna-Castroviejo, L. Qin, S.F. Yang, K. Xu, Melatonin, a full service anti-cancer agent: inhibition of initiation, progression and metastasis, Int. J. Mol. Sci. 18 (4) (2017) 843.

[40] R.J. Reiter, D.X. Tan, R.M. Sainz, J.C. Mayo, S. Lopez-Burillo, Melatonin: reducing the toxicity and increasing the efficacy of drugs, J. Pharm. Pharmacol. 54 (10) (2002) 1299–1321.

[41] X. Qiu, K. Brown, M.D. Hirschey, E. Verdin, D. Chen, Calorie restriction reduces oxidative stress by SIRT3-mediated SOD2 activation, Cell Metabol. 12 (6) (2010) 662–667.

[42] Y. Cheng, C. Dai, J. Zhang, SIRT3-SOD2-ROS pathway is involved in linalool-induced glioma cell apoptotic death, Acta Biochim. Pol. 64 (2) (2017) 343–350.

[43] R. Morabito, A. Remigante, A. Marino, Melatonin protects band 3 protein in human erythrocytes against H2O2-induced oxidative stress, Molecules 24 (15) (2019) 2741.
[44] S. Codenotti, M. Battistelli, S. Burattini, S. Salucci, E. Falcieri, R. Rezzani, F. Faggi, M. Colombi, E. Monti, A. Fanzani, Melatonin decreases cell proliferation, impairs myogenic differentiation and triggers apoptotic cell death in rhabdomyosarcoma cell lines, Oncol. Rep. 34 (1) (2015) 279–287.
[45] J.J. Lu, L. Fu, Z. Tang, C. Zhang, L. Qin, J. Wang, Z. Yu, D. Shi, X. Xiao, F. Xie, W. Huang, W. Deng, Melatonin inhibits AP-2beta/hTERT, NF-kappaB/COX-2 and Akt/ERK and activates caspase/Cyto C signaling to enhance the antitumor activity of berberine in lung cancer cells, Oncotarget 7 (3) (2016) 2985–3001.
[46] R.J. Youle, A. Strasser, The BCL-2 protein family: opposing activities that mediate cell death, Nat. Rev. Mol. Cell Biol. 9 (1) (2008) 47–59.
[47] D. Prabhavathy, C.K. Subramanian, D. Karunagaran, Re-expression of HPV16 E2 in SiHa (human cervical cancer) cells potentiates NF-kappaB activation induced by TNF-alpha concurrently increasing senescence and survival, Biosci. Rep. 35 (1) (2015), e00175.
[48] A. Cucina, S. Proietti, F. D'Anselmi, P. Coluccia, S. Dinicola, L. Frati, M. Bizzarri, Evidence for a biphasic apoptotic pathway induced by melatonin in MCF-7 breast cancer cells, J. Pineal Res. 46 (2) (2009) 172–180.
[49] S. Lin, K. Hoffmann, C. Gao, M. Petrulionis, I. Herr, P. Schemmer, Melatonin promotes sorafenib-induced apoptosis through synergistic activation of JNK/c-jun pathway in human hepatocellular carcinoma, J. Pineal Res. 62 (3) (2017), e12398.
[50] M. Bizzarri, S. Proietti, A. Cucina, R.J. Reiter, Molecular mechanisms of the pro-apoptotic actions of melatonin in cancer: a review, Expert Opin. Ther. Targets 17 (12) (2013) 1483–1496.
[51] R. Feng, W.L. Zhai, H.Y. Yang, H. Jin, Q.X. Zhang, Induction of ER stress protects gastric cancer cells against apoptosis induced by cisplatin and doxorubicin through activation of p38 MAPK, Biochem. Biophys. Res. Commun. 406 (2) (2011) 299–304.
[52] C. Kim, B. Kim, Anti-cancer natural products and their bioactive compounds inducing ER stress-mediated apoptosis: a review, Nutrients 10 (8) (2018) 1021.
[53] A. Fernandez, R. Ordonez, R.J. Reiter, J. Gonzalez-Gallego, J.L. Mauriz, Melatonin and endoplasmic reticulum stress: relation to autophagy and apoptosis, J. Pineal Res. 59 (3) (2015) 292–307.
[54] X. Han, K.A. Kang, M.J. Piao, A.X. Zhen, Y.J. Hyun, H.M. Kim, Y.S. Ryu, J.W. Hyun, Shikonin exerts cytotoxic effects in human colon cancers by inducing apoptotic cell death via the endoplasmic reticulum and mitochondria-mediated pathways, Biomol. Ther. (Seoul) 27 (1) (2019) 41–47.
[55] P. Wongprayoon, P. Govitrapong, Melatonin protects SH-SY5Y neuronal cells against methamphetamine-induced endoplasmic reticulum stress and apoptotic cell death, Neurotox. Res. 31 (1) (2017) 1–10.